

Magnetic Impurity in a Metal with Correlated Conduction Electrons: An Infinite Dimensions Approach

Benny Davidovich¹ and V. Zevin^{1,2}

¹*The Racah Institute of Physics, The Hebrew University of Jerusalem, 91904 Jerusalem, Israel*

²*Max-Planck-Institut für Physik Komplexer Systeme, Außenstelle Stuttgart,
Postfach 80 06 65, 70506 Stuttgart, Germany*

We consider the Hubbard model with a magnetic Anderson impurity coupled to a lattice site. In the case of infinite dimensions, one-particle correlations of the impurity electron are described by the effective Hamiltonian of the two-impurity system. One of the impurities interacts with a bath of free electrons and represents the Hubbard lattice, and the other is coupled to the first impurity by the bare hybridization interaction. A study of the effective two-impurity Hamiltonian in the frame of the $1/N$ expansion and for the case of a weak conduction-electron interaction (small U) reveals an enhancement of the usual exponential Kondo scale. However, an intermediate interaction ($U/D = 1 - 3$), treated by the variational principle, leads to the loss of the exponential scale. The Kondo temperature T_K of the effective two-impurity system is calculated as a function of the hybridization parameter and it is shown that T_K decreases with an increase of U . The non-Fermi-liquid character of the Kondo effect in the intermediate regime at the half filling is discussed.

PACS 71.10+w, 71.27+a, 75.20.Hr

I. INTRODUCTION

The physics of a magnetic impurity embedded in a metal with non-interacting conduction electrons is well now understood and documented [1,2]. Its characteristic feature is the many-body non-perturbative renormalization of the impurity-host interaction which turns to be strong at temperatures lower than the Kondo temperature T_K . This T_K is an exponential in the inverse impurity-host coupling parameter. Recently both the Kondo-spin model [3,4,5] and the Anderson impurity model were studied [6,7,8] in one-dimensional systems with interacting conduction electrons. It turns out that the influence of the conduction-electron interaction (CEI) on the Kondo effect [9] in a Luttinger liquid is not trivial: the Kondo screening of the impurity spin may also be possible for a ferromagnetic exchange coupling J [4,5]; for a sufficiently large CEI, a power-law dependence of T_K upon J replaces the usual exponential law [3,4,5]; in the case of the Anderson model a small CEI enhances T_K (just because more conduction electrons effectively participate in the interaction with an impurity) but this trend changes for a large enough CEI and T_K falls due to the suppression of the charge transfer between the impurity and the lattice [6,8]. A generalized Anderson impurity model for a Luttinger liquid which was introduced in [8] and studied there by the renormalization-group techniques

shows a rich phase diagram in the parameter space.

The interest in the Kondo effect in the interacting host for 2d and 3d was sparked by the discovery [10] of heavy-fermions in $Nd_{2-x}Ce_xCuO_4$ [11,12,13]. The Schrieffer-Wolff transformation for the magnetic impurity coupled to the Hubbard host was discussed in [14] and the Kondo-spin model in the above host was investigated in [15]. The Anderson impurity model for interacting conduction electrons was considered too. Its ground state energy was calculated in the frame of the $1/N$ expansion [16] and the Non-Crossing-Approximation (NCA) theory was generalized to the interacting case [17]. As was shown first in [15], two-particle Green's functions of host electrons (vertex corrections) are an essential ingredient of the correct theory of the Kondo effect in the interacting host. Actual calculations were carried out in the lowest order in the Hubbard U approximation and an enhancement of T_K [18] was obtained both for the Kondo-spin model [15] and the Anderson [16,17]. However, contrary to the 1d case, the theory of the Anderson impurity in 2d and 3d is not developed sufficiently beyond the case of the weak host interaction.

It is much easier to treat strongly interacting systems in the limit of infinite dimensions, $d \rightarrow \infty$ [19,20,21,22]. We use here the Local Impurity Self Consistent Approximation (LISA) [23,24,22] to map the Hubbard host with an Anderson impurity to a simpler model. As we show, this system is a two-impurity system in which one of the impurities represents the Hubbard host [22] and the other

is the original (bare) impurity coupled solely to the first impurity by the bare hybridization interaction. In the LISA approach the effective two-impurity Hamiltonian preserves all the features of the one particle Green's function of the impurity electron. Using for simplicity the Bethe lattice in its large connectivity limit, we show by employing the NCA for a weak CEI that the effective two-impurity Hamiltonian leads to an enhanced Kondo scale T_K in full agreement with [17,18]. For an intermediate CEI we solve the effective two-impurity Hamiltonian by using the variational principle, and calculate numerically the singlet and the triplet ground state energies. Their difference is no longer exponential in the inverse coupling parameter. For a small hybridization interaction it is linear in this parameter (i. e. in the Anderson width) and eventually exhibits a maximum. The latter appears at values of the Anderson width which are less than the impurity energy level. Moreover, in the intermediate range of CEI this difference decreases with the increase of U . This dependence of T_K upon the strength of CEI indicates that for intermediate values of U the suppression of the charge transfer between the impurity and host starts to be a dominant factor in the CEI influence on the singlet formation.

The paper is organized as follows: in section II the two-impurity effective Hamiltonian is derived, section III deals with a weak CEI and section IV is devoted to the intermediate one. Discussions and Conclusions are in section V.

II. THE EFFECTIVE TWO-IMPURITY HAMILTONIAN

We consider the Hubbard model with a magnetic impurity coupled to a lattice site. The Hamiltonian is

$$H = H_h + H_{imp} + H_{int} \quad (1)$$

The first term is the Hubbard Hamiltonian for the host lattice, the second is the impurity Hamiltonian and the third is the hybridization interaction between the impurity and the host. Figure 1 illustrates the system for the case of a Bethe lattice but the mapping discussed in this section is not limited to the Bethe type of lattice only. The Hubbard Hamiltonian for the host is

$$H_h = - \sum_{ij\sigma} (t_{ij} + \mu) c_{i\sigma}^\dagger c_{j\sigma} + \frac{U}{2} \sum_{i,\sigma \neq \sigma'} n_{i\sigma} n_{i\sigma'} \quad (2)$$

The operators $c_{i\sigma}^\dagger$ ($c_{i\sigma}$) create (annihilate) conduction electrons in spin states σ at site i and the corresponding density operators are $n_{i\sigma} = c_{i\sigma}^\dagger c_{i\sigma}$. The hopping between different sites i and j is given by t_{ij} , μ is the chemical potential while U is the Coulomb repulsion between two conduction electrons at the same site i . The impurity Hamiltonian is given by

$$H_{imp} = \sum_{\sigma} \epsilon_f n_{f\sigma} + \frac{U_f}{2} \sum_{\sigma \neq \sigma'} n_{f\sigma} n_{f\sigma'} \quad (3)$$

Here $n_{f\sigma} = f_{\sigma}^\dagger f_{\sigma}$ is the density operator for the impurity electron and f_{σ}^\dagger (f_{σ}) its creation (annihilation) operators. The impurity level ϵ_f is taken here relative to the chemical potential and the Coulomb repulsion between two f-electrons at the impurity site is U_f . The hybridization interaction is chosen in the simple form:

$$H_{int} = V \sum_{\sigma} (f_{\sigma}^\dagger c_{0\sigma} + h.c.) \quad (4)$$

and 0 denotes the lattice site to which the impurity is coupled. We will assume a half-filled case, $\langle n_{i\uparrow} \rangle = \langle n_{i\downarrow} \rangle = 1/2$. Our treatment of the Hamiltonian of Eq. (1) is based on the results of the LISA approach to the Hubbard model in infinite dimensions. Below we formulate some of the results which we use for the Anderson impurity in the Hubbard host.

A. A short overview of the LISA approach to the Hubbard model, $d \rightarrow \infty$

Following [22] we recall briefly the dynamical mean-field theory of the Hubbard model. In the limit of infinite dimensions the one-particle Green's function for the Hubbard Hamiltonian, Eq. (2), is local [20]:

$$G_{ij,\sigma}(i\omega_n) = \delta_{ij} G_{ii,\sigma}(i\omega_n) \quad (5)$$

and the usual definition

$$G_{ij,\sigma}(i\omega_n) = - \int_0^\beta d\tau \langle T c_{i,\sigma}(\tau) c_{j,\sigma}^\dagger(\tau') \rangle e^{i\omega_n(\tau - \tau')}$$

with $\omega_n = (2n+1)\pi\beta^{-1}$ is used everywhere. For the paramagnetic phase which is assumed in further discussions and in the absence of the f-impurity we may omit indices in the local Green's function of the Hubbard model, Eq. (5). The latter may be calculated by the means of the effective action S_{eff} :

$$S_{eff} = - \int_0^\beta d\tau \int_0^\beta d\tau' \sum_{\sigma} c_{0,\sigma}^\dagger(\tau) \mathcal{G}_0^{-1}(\tau - \tau') c_{0,\sigma}(\tau') + U \int_0^\beta d\tau n_{0\uparrow}(\tau) n_{0\downarrow}(\tau) \quad (6)$$

Here Grassmann variables are used and the effective action is obtained by tracing out all fermions except for a site labeled by 0 in the partition function:

$$e^{-S_{eff}} = \int \prod_{i \neq 0, \sigma} Dc_{i\sigma}^\dagger Dc_{i\sigma} e^{-S} \quad (7)$$

where S is the action of the Hubbard model, Eq. (2). The dynamic mean-field Green's function $\mathcal{G}_0(\tau - \tau')$, Eq. (6),

is connected to the local Green's function of the Hubbard model [22]. The latter may be calculated by the self-consistent iteration procedure via the use of the definition:

$$G(\tau - \tau') = \frac{\int \prod_{\sigma'} Dc_{0\sigma'}^\dagger Dc_{0\sigma'} e^{-S_{eff}} [-T c_{0\sigma}(\tau) c_{0\sigma}^\dagger(\tau')]}{\int \prod_{\sigma'} Dc_{0\sigma'}^\dagger Dc_{0\sigma'} e^{-S_{eff}}} \quad (8)$$

The dynamic mean-field Green's function \mathcal{G}_0 may be viewed as the bare Green's function of the impurity electron in the auxiliary Anderson impurity model [23,24,22]. In the latter the orbital $c_{0\sigma}^\dagger$ appears as the Anderson impurity and it possesses both the local energy level equal to $-\mu$ and the on-site Coulomb interaction equal to the same interaction as in the original Hubbard model, Eq. (1). This fictitious Anderson impurity (not to be confused with the original one in Eqs. (1-4)!) is coupled to a free-electron bath and the appropriate Hamiltonian reads [22]:

$$H_{AM} = \sum_{l\sigma} \tilde{\epsilon}_l a_{l\sigma}^\dagger a_{l\sigma} + \sum_{l\sigma} \mathcal{V}_l (a_{l\sigma}^\dagger c_{0\sigma} + h.c.) - \mu \sum_{\sigma} c_{0\sigma}^\dagger c_{0\sigma} + U n_{0\uparrow} n_{0\downarrow} \quad (9)$$

The action for the Hamiltonian H_{AM} is like S_{eff} in Eq. (6) with the dynamic mean-field Green's function $\mathcal{G}_0(\tau - \tau')$ given in the explicit form as a function of the parameters $\tilde{\epsilon}_l$ and \mathcal{V}_l . Using the Fourier transform of $\mathcal{G}_0(\tau - \tau')$ we have [22]

$$\mathcal{G}_0(i\omega_n) = \frac{1}{i\omega_n + \mu - \int_{-\infty}^{\infty} d\epsilon \frac{\Delta(\epsilon)}{i\omega_n - \epsilon}}; \quad \Delta(\epsilon) = \sum_{l\sigma} \mathcal{V}_l^2 \delta(\epsilon - \tilde{\epsilon}_l) \quad (10)$$

Due to the structure of the Bethe lattice which disconnects itself into two separate parts by removing a lattice site, the dependence between $\mathcal{G}_0(i\omega_n)$ and the local Green's function for the original Hubbard model $G(i\omega_n)$ is simplest. It may be shown [22] that

$$G(i\omega_n) = \frac{1}{t^2} \int_{-\infty}^{\infty} d\epsilon \frac{\Delta(\epsilon)}{i\omega_n - \epsilon} \quad (11)$$

Here the n.n. hopping is assumed in the Hamiltonian H_h , Eq. (2): $t_{ij} = t/\sqrt{d}$ for nearest neighbors and zero otherwise. Eqs. (10-11) together with Eq. (A8) permit to find $\Delta(\epsilon)$. For the non-interacting case, $U = 0$, the function $\Delta(\epsilon)/t^2$ is just the density of states of the Bethe lattice, $\rho(\epsilon)$ [22]:

$$\rho(\epsilon) = \frac{1}{\pi t} \sqrt{1 - \left(\frac{\epsilon}{2t}\right)^2}, \quad |\epsilon| \leq 2t \quad (12)$$

For finite values of U calculations were done in [25] (see also [22]) and Figure 2 from [25] illustrates results of these calculations. We are interested in the paramagnetic phase and to avoid Néel order a quenched disorder may be introduced in the n. n. hopping. The details are presented in [26,22] and we only note that by this generalisation neither the Bethe lattice semicircular density of states, Eq. (12), nor other local properties are changed.

B. The cavity method for the Anderson impurity in the Hubbard host

It is clear that the Anderson impurity being coupled to the site 0 destroys the equivalency between different sites of the Hubbard host. Let the index $i_m, m = 1, 2, \dots$ denotes one of equivalent neighbors of the site 0 on the Bethe lattice, m bonds away from it. Taking a site i_m as the "cavity place" for the dynamical mean-field treatment and tracing out all fermions but $c_{i_m}^\dagger$ the effective action $S_{eff}[c_{i_m}^\dagger c_{i_m}]$ may be calculated in close analogy with the pure Hubbard model. This action defines all local properties of the i_m -site and its form exactly as in Eq. (6) with the mean-field Green's function $\mathcal{G}_0^{(i_m)}(\tau - \tau')$ instead of the $\mathcal{G}_0(\tau - \tau')$. By straightforward calculations [27] it may be shown that

$$\mathcal{G}_0^{(i_1)}(i\omega_n) = i\omega_n + \mu + \sum_{\substack{i \text{ n.n. of } i_1 \\ i \neq 0}} \frac{t^2}{d} G_{ii}(i\omega_n) + \frac{t^2}{d} G_{00}(i\omega_n) \\ \mathcal{G}_0^{(i_m)}(i\omega_n) = i\omega_n + \mu + \sum_{i \text{ n.n. of } i_m} \frac{t^2}{d} G_{ii}(i\omega_n); m \neq 1 \quad (13)$$

It is obvious that for the case of infinite dimensions Eqs. (13) are solved by the $\mathcal{G}_0(i\omega_n)$ and $G(i\omega_n)$, Eqs. (10, 11) of the pure Hubbard model. In fact an impurity can not break the equivalency between different sites $i \neq 0$ of the Hubbard host and does not influence their local properties.

To calculate the correlation function of the impurity electron we trace out all fermions except two, $c_{0\sigma}^\dagger$ and f_σ^\dagger , in the partition function and define the effective action $S_{eff}[0, f]$:

$$e^{-S_{eff}[0, f]} = \int \prod_{i \neq 0, \sigma} Dc_{i\sigma}^\dagger Dc_{i\sigma} e^S \\ S = \int_0^\beta d\tau \left(\sum_{i\sigma} c_{i\sigma}^\dagger(\tau) \partial_\tau c_{i\sigma}(\tau) + \sum_{\sigma} f_\sigma^\dagger(\tau) \partial_\tau f_\sigma(\tau) + H_h(\tau) + H_{imp}(\tau) + H_{int}(\tau) \right) \quad (14)$$

Here H_h , H_{imp} , H_{int} are from Eqs. (2), (3), (4) respectively. Repeating the same calculations which lead to S_{eff}

of Eq. (6) for the Hubbard model without impurity [22], we obtain for the Bethe lattice of infinite connectivity

$$S_{eff}[0, f] = - \int_0^\beta d\tau \int_0^\beta d\tau' \sum_\sigma c_{0,\sigma}^\dagger(\tau) \mathcal{G}_0^{-1}(\tau - \tau') c_{0,\sigma}(\tau') + \int_0^\beta d\tau (U n_{0\uparrow}(\tau) n_{0\downarrow}(\tau) + \sum_\sigma f_\sigma^\dagger(\tau) \partial_\tau f_\sigma(\tau) + H_{imp}(\tau) + H_{int}(\tau)) \quad (15)$$

Note that here the dynamic mean-field Green's function $\mathcal{G}_0(\tau - \tau')$ coincides with the Green's function for the pure Hubbard model, Eq. (10).

To study the Kondo effect it is convenient to work with the effective Hamiltonian, $H_{eff}[0, f]$, which produces the same action as in Eq. (15). Because the Hubbard host is represented in Eq. (15) exactly like in the case of the Hubbard model without impurity it is easy to see that

$$H_{eff}[0, f] = H_{AM} + H_{imp} + H_{int}$$

. Using Eqs. (3), (4), (9) we obtain finally

$$H_{eff}[0, f] = \sum_{l\sigma} \tilde{\epsilon}_l a_{l\sigma}^\dagger a_{l\sigma} + \sum_{l\sigma} \mathcal{V}_l (a_{l\sigma}^\dagger c_{0\sigma} + h.c.) - \mu \sum_\sigma c_{0\sigma}^\dagger c_{0\sigma} + U n_{0\uparrow} n_{0\downarrow} + \sum_\sigma \epsilon_f n_{f\sigma} + \frac{U_f}{2} \sum_{\sigma \neq \sigma'} n_{f\sigma} n_{f\sigma'} + V \sum_\sigma (f_\sigma^\dagger c_{0\sigma} + h.c.) \quad (16)$$

The above Hamiltonian describes the two-impurity system in which the first one, $c_{0\sigma}^\dagger$, represents, together with the free-electron bath, the Hubbard host (see subsection II A) and the second impurity is coupled to the first one only. It is still a non-trivial model but because the influence of the impurity on the fitting set of parameters $\tilde{\epsilon}_l$ and \mathcal{V}_l is negligible we may use the function $\Delta(\epsilon)$, Eq. (10), as it is calculated for the Hubbard model. The function $\Delta(\epsilon)$ depends of course on the type of the lattice. In the following Section we consider the Kondo effect as it emerges from the Hamiltonian, Eq. (16), for the case of the Bethe lattice of infinite connectivity with the function $\Delta(\epsilon)$ taken from [25]. We assume that the energy U_f is much larger than other energetical scales in the problem and will take it infinitely large to exclude the double occupation of the impurity site.

III. WEAK CORRELATED HOST

To take into account the absence of double f-occupation we follow [28] and introduce the slave boson field b^\dagger, b with the restriction

$$b^\dagger b + \sum_\sigma c_{0\sigma}^\dagger c_{0\sigma} = 1 \quad (17)$$

The two-impurity Hamiltonian has to be modified in the well known fashion [28,29] and its form now is

$$H_{eff}[0, f, b] = \sum_{l\sigma} \tilde{\epsilon}_l a_{l\sigma}^\dagger a_{l\sigma} + \sum_{l\sigma} \mathcal{V}_l (a_{l\sigma}^\dagger c_{0\sigma} + h.c.) - \mu \sum_\sigma c_{0\sigma}^\dagger c_{0\sigma} + U n_{0\uparrow} n_{0\downarrow} + \sum_\sigma \epsilon_f n_{f\sigma} + \lambda b^\dagger b + V \sum_\sigma (f_\sigma^\dagger b c_{0\sigma} + h.c.) \quad (18)$$

Here λ is the slave boson chemical potential which in the final stage of calculations has to be put to $-\infty$ in order to satisfy the restriction of Eq. (17).

We begin with free electrons in the original Hamiltonian, Eq. (1), that is $U = 0$. Using the NCA in the lowest $1/N$ approximation the boson and f-pseudofermion self-energies may be calculated by the use of the Hamiltonian $H_{eff}[0, f, b]$ and compared with the well known results [28,29]. Figures 3 a, b depict these self-energies. The propagator of the first impurity electron in our two-impurity system (states $c_{0\sigma}^\dagger$) is labeled by $G_{AM}(i\omega_n)$. For $U = 0$ it is easy to calculate that

$$G_{AM}(i\omega_n) = \frac{1}{i\omega_n + \mu - \sum_l \frac{\mathcal{V}_l^2}{i\omega_n - \tilde{\epsilon}_l}} \quad (19)$$

The self-consistent mapping of the original system with $U = 0$ onto the two-impurity one means that the local Green's function $G(i\omega_n)$ coincides with $G_{AM}(i\omega_n)$. So we obtain

$$G_{AM}(i\omega_n) \equiv G(i\omega_n) = \int_{-\infty}^{\infty} d\epsilon \frac{\rho(\epsilon)}{i\omega_n - \epsilon + \mu} \quad (20)$$

Here $\rho(\epsilon)$ is the DOS of the host lattice, Eq. (2). Substituting in the expressions for the self-energies of Figures 3 a, b instead of the propagator $G_{AM}(i\omega_n)$ the Green's function $G(i\omega_n)$ from Eq. (20) one can recover, as it is expected for the non-interacting case, self-energy expressions as they emerge by the direct application of the NCA to the original Hamiltonian Eq. (1) [28,29]. The Kondo temperature T_K changes exponentially as a function of the coupling and in the lowest iteration of the NCA it has the form [30]

$$T_K = 2t \exp \frac{\pi \epsilon_f}{2\Gamma} \quad (21)$$

Here $\Gamma = \pi V^2 \rho(0)$ is the Anderson width.

The interaction case, $U \neq 0$, may also be considered in the frame of the NCA. In the lowest $1/N$ approximation the slave boson and f-pseudofermion self-energies acquire vertex corrections which take into account the CEI. These vertex corrections $\Gamma^U(1, 2; 3, 4)$ were discussed in [17] and shown in Figures 3 c, d. Now neither the propagator G_{AM} has the simple form of Eq. (19) nor G is of the non-interacting nature of Eq. (20). However, for

weak correlations the self-energies, Figures 3 c, d, may be calculated [17]. In this case of small U one may neglect the mass renormalization of band electrons [15] and use for G_{AM} Eq. (20), besides $\Gamma^U(1, 2; 3, 4) = U$. With these approximations the self-energies of Figures 3 c, d are exactly the same as calculated in [17] for the Hamiltonian, Eq. (1), in the usual three-dimensional case in the *local* approximation. According to [17] Eq. (21) is preserved (in the lowest iteration of the NCA) but the parameters ϵ_f and Γ undergo the renormalization (both $|\epsilon_f|$ and Γ increase linearly with U) leading to the enhancement of T_K . Details of this renormalization may be found in [17]. Note that in this section we did not use any specific properties of the Bethe lattice and its results are valid for any host lattice. It would be interesting to go in the NCA beyond the linear in the Hubbard U approximation but here we will apply the variational principle to handle the effective two-impurity Hamiltonian for intermedium values of U .

IV. INTERMEDIATE INTERACTIONS: VARIATIONAL APPROACH

By the intermediate interaction case we mean the range of the ratio $U/2t$ for which the host is still in the metallic regime, i.e. much before the metal-insulator transition takes place. From Figure 2 for the Bethe lattice which is considered throughout this section we take $U/2t \lesssim 3$ somewhat loosely for the upper limit. The lower limit in our case is dictated by the variational functions implemented here which put this limit at $U/2t \sim 1$ (see subsection IV B).

We construct here variational functions for the singlet and triplet states and find the ground singlet and lowest triplet energies. Essentially, we follow ideas of $1/N$ variational treatment of the Anderson impurity Hamiltonian developed in [31,32]. It is convenient to introduce a new representation for the bath states in Eq. (16):

$$\begin{aligned} \Psi_{\epsilon\sigma}^\dagger &= \mathcal{V}^{-1}(\epsilon) \sum_{l\sigma} \mathcal{V}_l^2 \delta(\epsilon - \tilde{\epsilon}_l) a_{l\sigma}^\dagger \\ \mathcal{V}(\epsilon) &\equiv \sqrt{\Delta(\epsilon)} \end{aligned} \quad (22)$$

Here $\Delta(\epsilon)$ is from Eq. (10). Using this definition the Hamiltonian $H_{eff}[0, f]$ may be rewritten as follows:

$$\begin{aligned} H_{eff}[0, f] &= \sum_{\sigma} \int d\epsilon (\epsilon \Psi_{\epsilon\sigma}^\dagger \Psi_{\epsilon\sigma} + \mathcal{V}(\epsilon) (\Psi_{\epsilon\sigma}^\dagger c_{0\sigma} + h.c.)) - \\ &\sum_{\sigma} (\mu n_{0,\sigma} - \epsilon_f n_{f\sigma}) + V \sum_{\sigma} (f_{\sigma}^\dagger c_{0\sigma} + h.c.) + \\ &U n_{0\uparrow} n_{0\downarrow} + \frac{U_f}{2} \sum_{\sigma \neq \sigma'} n_{f\sigma} n_{f\sigma'} \end{aligned} \quad (23)$$

Note that since $\mu = U/2$ the c_0 -impurity is described by the symmetric Anderson model while the double occupancy of the f-level is forbidden ($U_f \rightarrow \infty$).

A. Variational functions

Figure 4 schematically represents the singlet state variational function. We have two groups of states: one contains four states in which the f-level is unoccupied, the other is of six states in which the f-level is singly occupied. For vanishing hybridization coupling $V = 0$ two groups are decoupled and the first one is just the variational function of the symmetric Anderson impurity. We want to keep only the lowest contributions in $1/N$ which come from the states without electron-hole pairs [31,32]. For the symmetrical Anderson impurity the occupation of the empty state has to equal that of the doubly-occupied one which may be achieved only by including states with one electron-hole pair at least [32]. We included only one such state (ϕ_3 in Figure 4) and we checked that the four-state variational function for the symmetric Anderson impurity produces the required equality between occupancies of the empty and doubly-occupied states. There are two additional states with one electron-hole pair [32]. Including them, however, would make calculations too cumbersome. Being interested in the qualitative influence of the Hubbard U on the Kondo effect we limited ourselves to the lowest possible combination of states which is expected to give correct qualitative results at least. The second group of states (states 4 - 9 in Figure 4) are chosen from the same considerations.

We denote states by ϕ_i , $i = 0, 1, \dots, 9$, so $\phi_0 = |0\rangle$ represents the vacuum (full Fermi sea and empty local states), $\phi_1(\epsilon) = 1/\sqrt{2} \sum_{\sigma} \Psi_{\epsilon,\sigma}^\dagger c_{0\sigma}^\dagger |0\rangle$, \dots , $\phi_9(\epsilon_1, \epsilon_2, E) = 1/\sqrt{2} \sum_{\sigma} \Psi_{\epsilon_1,\sigma}^\dagger \Psi_{\epsilon_2,\sigma}^\dagger \Psi_{E,\sigma}^\dagger f_{\sigma}^\dagger |0\rangle$. All ϕ -functions are listed in the Appendix A. In this basis the singlet ground state of the Hamiltonian Eq. (23) has the following form:

$$\begin{aligned} \psi_s &= \mathcal{N} [\phi_0 + \int_{-D}^0 d\epsilon_1 (\\ &r_1(\epsilon_1) \phi_1 + \int_{-D}^{\epsilon_1} d\epsilon_2 r_2(\epsilon_1, \epsilon_2) \phi_2 + \int_0^D dE r_3(\epsilon_1, E) \phi_3 + \\ &r_4(\epsilon_1) \phi_4 + \int_{-D}^0 d\epsilon_2 r_5(\epsilon_1, \epsilon_2) \phi_5 + \int_0^{\epsilon_1} d\epsilon_2 r_6(\epsilon_1, \epsilon_2) \phi_6 + \\ &\int_{-D}^{\epsilon_1} d\epsilon_2 \int_D^0 d\epsilon_3 r_7(\epsilon_1, \epsilon_2, \epsilon_3) \phi_7 + \int_{-D}^0 d\epsilon_2 \int_0^D dE r_8(\epsilon_1, \epsilon_2, E) \phi_8 \\ &+ \int_{-D}^{\epsilon_1} d\epsilon_2 \int_0^D dE r_9(\epsilon_1, \epsilon_2, E) \phi_9)] \end{aligned} \quad (24)$$

Here \mathcal{N} is the normalization factor and r_i are superposition functions which have to be determined by the energy minimization. For convenience, the energies of free electrons are denoted here by ϵ for a negative part of their spectrum and by E for the positive part and $D \equiv 2t$. Because the replacement $\epsilon_1 \leftrightarrow \epsilon_2$ for $\phi_2(\epsilon_1, \epsilon_2)$, $\phi_6(\epsilon_1, \epsilon_2)$ and $\phi_9(\epsilon_1, \epsilon_2, E)$ does not give new independent functions the upper limit of appropriate inner integrals is equal to ϵ_1 . The first four out of ten integral equations connecting different r_i , $i = 0, 1, \dots, 9$ are

$$r_0 = \frac{\int_{-D}^0 d\epsilon r_1(\epsilon)}{\Delta E_s} \quad (25)$$

and

$$\begin{aligned} r_1(\epsilon) &= [V r_2(\epsilon) + \sqrt{2}\mathcal{V}(\epsilon)r_0 + \int_{-D}^0 d\epsilon_1 \mathcal{V}(\epsilon_1) \tilde{r}_2(\epsilon, \epsilon_1) + \\ &\quad \int_0^D dE \mathcal{V}(E) r_2(\epsilon, E)] / (\Delta E_s + \epsilon + \mu) \\ \tilde{r}_2(\epsilon, \epsilon_1) &= [\mathcal{V}(\epsilon_1) r_1(\epsilon_2) + \mathcal{V}(\epsilon_2) r_1(\epsilon_1) + \\ &\quad V(r_5(\epsilon_1, \epsilon_2) + r_5(\epsilon_2, \epsilon_1))] / (\Delta E_s + \epsilon_1 + \epsilon_2) \\ r_3(\epsilon, E) &= \mathcal{V}(E) r_1(\epsilon) / (\Delta E_s + \epsilon - E) \end{aligned} \quad (26)$$

while the rest of the integral equations may be found in Appendix B. Here ΔE_s is the energy difference between the singlet ground state energy and the energy of the filled Fermi sea of the effective conduction band, Eq.(23); $\tilde{r}_2(\epsilon, \epsilon_1) = r_2(\epsilon, \epsilon_1)$ if $\epsilon \geq \epsilon_1$ and $\tilde{r}_2(\epsilon, \epsilon_1) = r_2(\epsilon_1, \epsilon)$ if $\epsilon \leq \epsilon_1$. Before we proceed with the numeric variational calculations let us discuss the variational functions for magnetic states.

We consider triplet, $S = 1$, states. Because of the rotational symmetry it is sufficient for our purposes to deal with the state of $S_z = 1$. The basis of this state may be generated from the singlet basis of Appendix A by applying to them the operator $\Psi_{\epsilon\downarrow} c_{0\uparrow}^\dagger$. The magnetic basis consists of functions $\Phi_i, i = 1, \dots, 12$ and the first three are $\Phi_1(\epsilon) = \Psi_{\epsilon\downarrow} c_{0\uparrow}^\dagger |0\rangle$, $\Phi_2(\epsilon_1, \epsilon_2) = \Psi_{\epsilon_1\downarrow} \Psi_{\epsilon_2\downarrow} c_{0\uparrow}^\dagger |0\rangle$ and $\Phi_3(\epsilon, E) = \Psi_{\epsilon\downarrow} \Psi_{E\uparrow}^\dagger |0\rangle$. These three states compose the $S_z = 1$ state of the symmetric Anderson impurity when it is decoupled from the rest of the system, Eq. (23). Other basis states are written in Appendix A. The triplet $S_z = 1$ variational function therefore reads:

$$\begin{aligned} \psi_t &= \mathcal{N} \left[\int_{-D}^0 d\epsilon_1 (\right. \\ &R_1(\epsilon_1) \Phi_1 + \int_{-D}^{\epsilon_1} d\epsilon_2 R_2(\epsilon_1, \epsilon_2) \Phi_2 + \int_0^D dE R_3(\epsilon_1, E) \Phi_3 + \\ &R_4(\epsilon_1) \Phi_4 + \int_{-D}^{\epsilon_1} d\epsilon_2 R_5(\epsilon_1, \epsilon_2) \Phi_5 + \int_{-D}^0 d\epsilon_2 R_6(\epsilon_1, \epsilon_2) \Phi_6 + \\ &\int_{-D}^{\epsilon_1} d\epsilon_2 R_7(\epsilon_1, \epsilon_2) \Phi_7 + \int_{-D}^0 d\epsilon_2 \int_{-D}^{\epsilon_1} d\epsilon_3 R_8(\epsilon_1, \epsilon_2, \epsilon_3) \Phi_8 + \\ &\int_{-D}^{\epsilon_1} d\epsilon_2 \int_{-D}^{\epsilon_2} d\epsilon_3 R_9(\epsilon_1, \epsilon_2, \epsilon_3) \Phi_9 + \\ &\int_{-D}^{\epsilon_1} d\epsilon_2 \int_0^D dE R_{10}(\epsilon_1, \epsilon_2, E) \Phi_{10} + \\ &\int_{-D}^0 d\epsilon_2 \int_0^D dE R_{11}(\epsilon_1, \epsilon_2, E) \Phi_{11} + \\ &\left. \int_{-D}^{\epsilon_1} d\epsilon_2 \int_0^D dE R_{12}(\epsilon_1, \epsilon_2, E) \Phi_{12} \right] \end{aligned} \quad (27)$$

Here upper limits of some integrals are chosen to avoid double counting of states and functions R_i must be obtained from the minimization of the triplet energy. As it

is seen from the list of the functions in Appendix A the $S_z = 1$ basis is composed from three groups of states. The first group contains the above written symmetric Anderson impurity states, in the two others the real impurity level is occupied, the difference between the second and the third group being the origin of the triplet. In the second the triplet originates from the real impurity and a conduction electron and in the third group it is from the symmetric Anderson impurity and a conduction electron. Integral equations which connect different functions R_i are collected in Appendix B. In the next subsection we suggest an effective numerical iteration method which was implemented here for carrying out the energy minimization both for the singlet and for the triplet.

B. An iteration method for the energy minimization and results

The direct numerical diagonalization of the two systems of linear integral equations, Eqs. (25), (26), (B1 - B6) for the singlet state and (B11 - B22) for the magnetic state, would be a very time consuming task. To find the energy shift ΔE_s together with the r_i functions we solve the integral equations system of Eqs. (25), (26), (B1 - B6) numerically for an arbitrary given value of ΔE_s , say ΔE . This is done by the controlled iteration procedure which starts with a most reasonable guess about the initial r_i functions. A fast convergence is usually obtained by choosing all but two initial r_i equal to zero and by selecting these two from states which are expected to contribute significantly to the superposition ψ_s . Let $r_i^{\Delta E}$ are functions calculated in the above procedure. Then we obtain by the use of Eq. (25) the following function $f(\Delta E)$:

$$f(\Delta E) \equiv \frac{\int_{-D}^0 d\epsilon r_1^{\Delta E}(\epsilon)}{r_0^{\Delta E}} \quad (28)$$

In view of the arbitrariness of ΔE , $f(\Delta E)$ does not coincide with ΔE , the equality between them is realized by ΔE_s (see Eq. (25)). So the latter may be seen as a minimal possible fixed point of the function f , Eq. (28):

$$f(\Delta E_s) = \Delta E_s.$$

This fixed point may be found after a few trials. Note that this scheme does not require the normalization of the ψ_s , Eq.(24), to be fulfilled in each stage of iterations. To find the energy shift ΔE_t between the lowest magnetic state and the energy of the filled Fermi sea of the conduction band of Eq. (23) the analogical iteration method is applied to the above magnetic state, Eq. (27). An illustration of the iteration procedure and some details of it are given in Appendix C.

It is clear from general considerations that values of U here have to be limited from below just because of the restricted basis which is used (see Figure 4). In addition,

in our case we are interested in the Kondo limit of almost filled states ϕ_5 and ϕ_6 . Therefore the local energy $U/2$ of the Anderson impurity with states $c_{0,\sigma}^\dagger$ in the two-impurity Hamiltonian, Eq. (23), has to be much larger than the maximal coupling parameter $\Gamma_1 = \pi\mathcal{V}^2(0)$. By the definition of $\mathcal{V}(\epsilon)$, Eq. (22), this gives :

$$U/D \gg 1/4$$

The hybridization coupling parameter for the real impurity in the two-impurity Hamiltonian, Eq. (23), may be defined in the usual way from the original Hamiltonian, Eq. (1), as the Anderson width $\Gamma = \pi V^2 \rho(0)$ with $\rho(0) = 2/\pi D$ (see Figure 2). The Kondo limit for the real impurity is given then by the condition:

$$|\epsilon_f| > 2V^2/D.$$

Two values of $\epsilon_f/D = -0.67$ and -0.3 were used in our calculations. Figure 5 presents the dependence of the energy difference $T_K = \Delta E_t - \Delta E_s$ on V^2 for both values of ϵ_f and $U/D = 1$ as calculated by the described above iteration method.

Figure 6 compares T_K as a function of V^2 for different values of U and $\epsilon_f/D = -0.3$. Figure 7 illustrates the decrease of T_K with the U increase. Here for the comparison the standard Kondo temperature from Eq. (21) is also shown.

V. DISCUSSIONS AND CONCLUSIONS

Summarizing the above we note that i) weak coupling between conduction electrons does not destroy the usual exponential Kondo scale (for $\Gamma \ll \epsilon_f$) but renormalizes the parameters Γ and ϵ_f ; ii) the exponential scale of T_K is lost already for $U/D = 1$. Moreover, for small Γ the Kondo temperature T_K is proportional to V^2 (see Figures 5 and 6); iii) there is a pronounced maximum on Figure 6 for $U = 2, 2.5$ and an indication on a broad one in Figure 5 for $U = 1$ and iv) in the range of $U \geq D$ the T_K decreases with the increase of U .

The enhancement of T_K in the Kondo regime by a weak coupling between conduction electrons is understood (see [15,17]) and is caused by the reduced probability of finding doubly occupied and empty lattice sites in the correlated system. This leads to the increased number of uncompensated conduction electron spins and to increase of the effective hybridisation. Our two-impurity model for $d \rightarrow \infty$ gives just the same result.

The loss of the exponential scale for intermediate $U/D = 2$ and 2.5 does not come as a surprise because for these values the DOS of Figure 2 has the typical three peak structure of the Anderson impurity and the Hubbard host excitations in this case are not of the Fermi-liquid character [22]. However, for $U = 1$ there are no gaps in the DOS and ϵ_f lies within the metallic looking DOS. Nevertheless also this case is qualitatively different from the non-interacting one. This difference can

be seen in the frame of our two-impurity model. Indeed when the real impurity is decoupled, $V = 0$, the rest of the system is just the symmetric Anderson impurity embedded in the bath. At $T = 0$ and provided that $U \gg \Gamma_1$ this system possesses the Kondo temperature which may be viewed as the energy difference between the ground singlet and lowest relevant magnetic states [34] of the symmetric Anderson model. This Kondo temperature for the symmetric Anderson impurity is referred to as T_K^{AM} and it was calculated in Appendix C for several values of U (see Appendix C). By coupling the real Anderson impurity to the system with a precursory non-zero energy difference between the ground singlet and the lowest relevant magnetic states we may expect for small coupling $2V^2/D \ll T_K^{AM}$ a perturbative linear dependence between T_K and V^2 . Using values of T_K^{AM} from Appendix C we obtain regions of linear dependence which are in a fair agreement with Figures 5 and 6. For small enough $U < \Gamma_1$ the symmetric Anderson impurity enters in the non-magnetic regime of the resonance level (see [1]). Using $\Gamma_1 = \pi\mathcal{V}^2(0)$ and Eqs. (12) and (22) we see that this happens at $U/D \sim 1/2$ and we expect that the usual Fermi-liquid picture of the Kondo effect emerges below this value of U/D . Unfortunately, as was discussed in the subsection IV B, we cannot treat this region of smaller U in the frame of the above variational approach. So the physics of the crossover from the Fermi-liquid regime with the exponential Kondo scale to the new regime where the Kondo exponential scale is lost is waiting for further investigations, perhaps in the frame of the diagrammatic approach but beyond the weak coupling which was discussed in Section III.

In general a non-monotonic behaviour of T_K as a function of V^2 may be expected at $\Gamma \lesssim |\epsilon_f|$ when the transition from the Kondo regime to the mixed valence regime occurs [35]. The maximum of the upper curve with $|\epsilon_f| = 0.3$, Figure 5, occurs at $\Gamma = 2V^2/D \sim 0.2$, and is in accordance with this expectation. However the lower curve of this figure which corresponds to the same $U/D = 1$ and about twice larger $|\epsilon_f|$ seems to saturate in the same region as the upper curve. In view of the specific form of the DOS of Figure 2 one has to be cautious to directly use the criteria taken from the non-interacting case. It is especially true for the cases of larger $U = 2, 2.5$ and $\epsilon_f = -0.3$ on Figure 6. The maximum appears there at $\Gamma \sim 0.1$ and 0.04 correspondingly showing a strong dependence of T_K upon U . In both last cases the local bare level ϵ_f is on the edge of the central portion of DOS, Figure 2, which narrows much with U . This narrowing of DOS determines the U -dependence of T_K .

The decrease of T_K as U increases is expected for sufficiently large U because the charge transfer from the impurity to the lattice eventually will be inhibited by the energy cost of the double occupancy of the lattice sites. The most interesting region of U values, where the cross-over from the exponential Kondo scale to the perturbative one takes place, has yet to be explored. It

would be desirable to study the entire range of U by one method of treatment. It would be interesting also to look into the experimental aspects of the Kondo effect as a tool for detecting non-Fermi-liquid properties of a strongly correlated metal.

In conclusion, we reduced the treatment of the Kondo effect in the Hubbard host of infinite dimensions to study of a simpler two-impurity Hamiltonian. The weakly correlated case was treated by the NCA and relations to previous studies of the Anderson impurity in a correlated host in 2d and 3d were shown. The variational treatment of the two-impurity Hamiltonian for intermediate interactions reveals a non-exponential behaviour of the Kondo scale and qualitative explanations for this behavior were proposed.

VI. ACKNOWLEDGEMENT

This work was supported by the Israel Science Foundation administered by the Israel Academy of Sciences and Humanities. V. Z. is grateful to the Max-Planck-Institute PKS for hospitality. The authors would like to thank G. Kotliar for education in the LISA during his lectures in Jerusalem and M. Rozenberg for sending to us his numeric data of DOS of the Hubbard model on the Bethe lattice. Useful discussions with G. Khaliullin and G. Zwicknagl are acknowledged.

APPENDIX A: TABLES OF FUNCTIONS

The basis of the singlet ground state, Eq. (24), follows:

$$\phi_0 = |0\rangle \quad (\text{A1})$$

$$\phi_1(\epsilon) = \frac{1}{\sqrt{2}} \sum_{\sigma} \Psi_{\epsilon\sigma} c_{0\sigma}^{\dagger} |0\rangle \quad (\text{A2})$$

$$\phi_2(\epsilon_1, \epsilon_2) = \frac{1}{\sqrt{2}} \sum_{\sigma} \Psi_{\epsilon_1\sigma} \Psi_{\epsilon_2-\sigma} c_{0\sigma}^{\dagger} c_{0-\sigma}^{\dagger} |0\rangle \quad (\text{A3})$$

$$\phi_3(\epsilon, E) = \frac{1}{\sqrt{2}} \sum_{\sigma} \Psi_{\epsilon\sigma} \Psi_{E\sigma}^{\dagger} |0\rangle \quad (\text{A4})$$

$$\phi_4(\epsilon) = \frac{1}{\sqrt{2}} \sum_{\sigma} \Psi_{\epsilon\sigma} f_{\sigma}^{\dagger} |0\rangle \quad (\text{A5})$$

$$\phi_5(\epsilon_1, \epsilon_2) = \frac{1}{\sqrt{2}} \sum_{\sigma} \Psi_{\epsilon_1\sigma} \Psi_{\epsilon_2-\sigma} c_{0-\sigma}^{\dagger} f_{\sigma}^{\dagger} |0\rangle \quad (\text{A6})$$

$$\phi_6(\epsilon_1, \epsilon_2) = \frac{1}{\sqrt{2}} \sum_{\sigma} \Psi_{\epsilon_1\sigma} \Psi_{\epsilon_2\sigma} c_{0\sigma}^{\dagger} f_{\sigma}^{\dagger} |0\rangle \quad (\text{A7})$$

$$\phi_7(\epsilon_1, \epsilon_2, \epsilon_3) = \frac{1}{\sqrt{2}} \sum_{\sigma} \Psi_{\epsilon_1\sigma} \Psi_{\epsilon_2\sigma} \Psi_{\epsilon_3-\sigma} c_{0\sigma}^{\dagger} c_{0-\sigma}^{\dagger} f_{\sigma}^{\dagger} |0\rangle \quad (\text{A8})$$

$$\phi_8(\epsilon_1, \epsilon_2, E) = \frac{1}{\sqrt{2}} \sum_{\sigma} \Psi_{\epsilon_1\sigma} \Psi_{\epsilon_2-\sigma} \Psi_{E-\sigma}^{\dagger} f_{\sigma}^{\dagger} |0\rangle \quad (\text{A9})$$

$$\phi_9(\epsilon_1, \epsilon_2, E) = \frac{1}{\sqrt{2}} \sum_{\sigma} \Psi_{\epsilon_1\sigma} \Psi_{\epsilon_2\sigma} \Psi_{E\sigma}^{\dagger} f_{\sigma}^{\dagger} |0\rangle \quad (\text{A10})$$

Beneath is the basis of the magnetic state, Eq. (27):

$$\Phi_1(\epsilon) = \Psi_{\epsilon\downarrow} c_{0\uparrow}^{\dagger} |0\rangle \quad (\text{A11})$$

$$\Phi_2(\epsilon_1, \epsilon_2) = \Psi_{\epsilon_1\downarrow} \Psi_{\epsilon_2\downarrow} c_{0\downarrow}^{\dagger} c_{0\uparrow}^{\dagger} |0\rangle \quad (\text{A12})$$

$$\Phi_3(\epsilon, E) = \Psi_{\epsilon\downarrow} \Psi_{E\uparrow}^{\dagger} |0\rangle \quad (\text{A13})$$

$$\Phi_4(\epsilon) = \Psi_{\epsilon\downarrow} f_{\uparrow}^{\dagger} |0\rangle \quad (\text{A14})$$

$$\Phi_5(\epsilon_1, \epsilon_2) = \Psi_{\epsilon_1\downarrow} \Psi_{\epsilon_2\downarrow} c_{0\downarrow}^{\dagger} f_{\uparrow}^{\dagger} |0\rangle \quad (\text{A15})$$

$$\Phi_6(\epsilon_1, \epsilon_2) = \Psi_{\epsilon_1\downarrow} \Psi_{\epsilon_2\uparrow} c_{0\uparrow}^{\dagger} f_{\uparrow}^{\dagger} |0\rangle \quad (\text{A16})$$

$$\Phi_7(\epsilon_1, \epsilon_2) = \Psi_{\epsilon_1\downarrow} \Psi_{\epsilon_2\downarrow} c_{0\uparrow}^{\dagger} f_{\downarrow}^{\dagger} |0\rangle \quad (\text{A17})$$

$$\Phi_8(\epsilon_1, \epsilon_2, \epsilon_3) = \Psi_{\epsilon_1\downarrow} \Psi_{\epsilon_2\uparrow} \Psi_{\epsilon_3\downarrow} c_{0\downarrow}^{\dagger} c_{0\uparrow}^{\dagger} f_{\uparrow}^{\dagger} |0\rangle \quad (\text{A18})$$

$$\Phi_9(\epsilon_1, \epsilon_2, \epsilon_3) = \Psi_{\epsilon_1\downarrow} \Psi_{\epsilon_2\downarrow} \Psi_{\epsilon_3\downarrow} c_{0\downarrow}^{\dagger} c_{0\uparrow}^{\dagger} f_{\downarrow}^{\dagger} |0\rangle \quad (\text{A19})$$

$$\Phi_{10}(\epsilon_1, \epsilon_2, E) = \Psi_{\epsilon_1\downarrow} \Psi_{\epsilon_2\downarrow} \Psi_{E\downarrow}^{\dagger} f_{\uparrow}^{\dagger} |0\rangle \quad (\text{A20})$$

$$\Phi_{11}(\epsilon_1, \epsilon_2, E) = \Psi_{\epsilon_1\downarrow} \Psi_{\epsilon_2\uparrow} \Psi_{E\uparrow}^{\dagger} f_{\uparrow}^{\dagger} |0\rangle \quad (\text{A21})$$

$$\Phi_{12}(\epsilon_1, \epsilon_2, E) = \Psi_{\epsilon_1\downarrow} \Psi_{\epsilon_2\downarrow} \Psi_{E\uparrow}^{\dagger} f_{\downarrow}^{\dagger} |0\rangle \quad (\text{A22})$$

APPENDIX B: INTEGRAL EQUATIONS

The equations for the functions r_4, \dots, r_9 are

$$\begin{aligned} r_4(\epsilon) = [& V r_1(\epsilon) \\ & + \int_{-D}^0 d\epsilon_1 \mathcal{V}(\epsilon_1) [r_5(\epsilon, \epsilon_1) \\ & + \tilde{r}_6(\epsilon, \epsilon_1)]] / (\Delta E_s + \epsilon - \epsilon_f) \end{aligned} \quad (\text{B1})$$

$$\begin{aligned} r_5(\epsilon_1, \epsilon_2) = [& V \tilde{r}_2(\epsilon_1, \epsilon_2) \\ & + \mathcal{V}(\epsilon_2) r_4(\epsilon_1) + \int_{-D}^0 d\epsilon_3 \mathcal{V}(\epsilon_3) \tilde{r}_7(\epsilon_1, \epsilon_3, \epsilon_2) \\ & + \int_0^D dE \mathcal{V}(E) r_8(\epsilon_1, \epsilon_2, E)] \\ & / (\Delta E_s + \epsilon_1 + \epsilon_2 + \mu - \epsilon_f) \end{aligned} \quad (\text{B2})$$

$$\begin{aligned} \tilde{r}_6(\epsilon_1, \epsilon_2) = [& \mathcal{V}(\epsilon_1) r_4(\epsilon_2) + \mathcal{V}(\epsilon_2) r_4(\epsilon_1) \\ & + \int_{-D}^0 d\epsilon_3 \mathcal{V}(\epsilon_3) \tilde{r}_4(\epsilon_1, \epsilon_2, \epsilon_3) \\ & + \int_0^D dE \mathcal{V}(E) \tilde{r}_9(\epsilon_1, \epsilon_2, E)] \\ & / (\Delta E_s + \epsilon_1 + \epsilon_2 + \mu - \epsilon_f) \end{aligned} \quad (\text{B3})$$

$$\begin{aligned} \tilde{r}_7(\epsilon_1, \epsilon_2, \epsilon_3) = [& \mathcal{V}(\epsilon_1) r_5(\epsilon_1, \epsilon_2) + \mathcal{V}(\epsilon_2) r_5(\epsilon_1, \epsilon_3) \\ & + \mathcal{V}(\epsilon_3) \tilde{r}_6(\epsilon_1, \epsilon_2)] \\ & / (\Delta E_s + \epsilon_1 + \epsilon_2 + \epsilon_3 - \epsilon_f) \end{aligned} \quad (\text{B4})$$

$$r_8(\epsilon_1, \epsilon_2, E) = \mathcal{V}(E) r_5(\epsilon_1, \epsilon_2)$$

$$/ (\Delta E_s + \epsilon_1 + \epsilon_2 - E - \epsilon_f) \quad (\text{B5})$$

$$\begin{aligned} \tilde{r}_9(\epsilon_1, \epsilon_2, E) &= \mathcal{V}(E) \tilde{r}_6(\epsilon_1, \epsilon_2) \\ &/ (\Delta E_s + \epsilon_1 + \epsilon_2 - E - \epsilon_f). \end{aligned} \quad (\text{B6})$$

where

$$\begin{aligned} \tilde{r}_2(\epsilon_1, \epsilon_2) &= \Theta(\epsilon_1 - \epsilon_2) r_2(\epsilon_1, \epsilon_2) \\ &+ \Theta(\epsilon_2 - \epsilon_1) r_2(\epsilon_2, \epsilon_1) \end{aligned} \quad (\text{B7})$$

$$\begin{aligned} \tilde{r}_6(\epsilon_1, \epsilon_2) &= \Theta(\epsilon_1 - \epsilon_2) r_6(\epsilon_1, \epsilon_2) \\ &+ \Theta(\epsilon_2 - \epsilon_1) r_6(\epsilon_2, \epsilon_1) \end{aligned} \quad (\text{B8})$$

$$\begin{aligned} \tilde{r}_7(\epsilon_1, \epsilon_2, \epsilon_3) &= \Theta(\epsilon_1 - \epsilon_2) r_7(\epsilon_1, \epsilon_2, \epsilon_3) \\ &+ \Theta(\epsilon_2 - \epsilon_1) r_7(\epsilon_2, \epsilon_1, \epsilon_3) \end{aligned} \quad (\text{B9})$$

$$\begin{aligned} \tilde{r}_9(\epsilon_1, \epsilon_2, E) &= \Theta(\epsilon_1 - \epsilon_2) r_9(\epsilon_1, \epsilon_2, E) \\ &+ \Theta(\epsilon_2 - \epsilon_1) r_9(\epsilon_2, \epsilon_1, E). \end{aligned} \quad (\text{B10})$$

The equations for the functions R_1, \dots, R_{12} are

$$\begin{aligned} R_1(\epsilon) &= [V R_4(\epsilon) \\ &+ \int_{-D}^0 d\epsilon_1 \mathcal{V}(\epsilon_1) \tilde{R}_2(\epsilon, \epsilon_1) \\ &+ \int_0^D dE \mathcal{V}(E) d(\epsilon, E)] \\ &/ (\Delta E_t + \epsilon + \mu) \end{aligned} \quad (\text{B11})$$

$$\begin{aligned} \tilde{R}_2(\epsilon_1, \epsilon_2) &= [\mathcal{V}(\epsilon_1) R_1(\epsilon_2) + \mathcal{V}(\epsilon_2) R_1(\epsilon_1) \\ &+ V [\tilde{R}_5(\epsilon_1, \epsilon_2) + \tilde{R}_7(\epsilon_1, \epsilon_2)]] \\ &/ (\Delta E_t + \epsilon_1 + \epsilon_2) \end{aligned} \quad (\text{B12})$$

$$R_3(\epsilon, E) = \mathcal{V}(E) R_1(\epsilon) / (\Delta E_t + \epsilon - E) \quad (\text{B13})$$

$$\begin{aligned} R_4(\epsilon) &= [V R_1(\epsilon) \\ &+ \int_{-D}^0 d\epsilon_1 \mathcal{V}(\epsilon_1) [\tilde{R}_5(\epsilon, \epsilon_1) \\ &+ R_6(\epsilon, \epsilon_1)]] \\ &/ (\Delta E_t + \epsilon - \epsilon_f) \end{aligned} \quad (\text{B14})$$

$$\begin{aligned} \tilde{R}_5(\epsilon_1, \epsilon_2) &= [V \tilde{R}_2(\epsilon_1, \epsilon_2) \\ &+ \mathcal{V}(\epsilon_2) R_4(\epsilon_1) + \mathcal{V}(\epsilon_1) R_4(\epsilon_2) \\ &+ \int_{-D}^0 d\epsilon_3 \mathcal{V}(\epsilon_3) \tilde{R}_8(\epsilon_1, \epsilon_3, \epsilon_2) \end{aligned}$$

$$\begin{aligned} &+ \int_0^D dE \mathcal{V}(E) \tilde{R}_{10}(\epsilon_1, \epsilon_2, E)] \\ &/ (\Delta E_t + \epsilon_1 + \epsilon_2 + \mu - \epsilon_f) \end{aligned} \quad (\text{B15})$$

$$\begin{aligned} R_6(\epsilon_1, \epsilon_2) &= [\mathcal{V}(\epsilon_2) R_4(\epsilon_1) \\ &+ \int_{-D}^0 d\epsilon_3 \mathcal{V}(\epsilon_3) \tilde{R}_8(\epsilon_1, \epsilon_2, \epsilon_3) \\ &+ \int_0^D dE \mathcal{V}(E) R_{11}(\epsilon_1, \epsilon_2, E)] \\ &/ (\Delta E_t + \epsilon_1 + \epsilon_2 + \mu - \epsilon_f) \end{aligned} \quad (\text{B16})$$

$$\begin{aligned} \tilde{R}_7(\epsilon_1, \epsilon_2) &= [V \tilde{R}_2(\epsilon_1, \epsilon_2) \\ &+ \int_{-D}^0 d\epsilon_3 \mathcal{V}(\epsilon_3) \tilde{R}_9(\epsilon_1, \epsilon_2, \epsilon_3) \\ &+ \int_0^D dE \mathcal{V}(E) \tilde{R}_{12}(\epsilon_1, \epsilon_2, E)] \\ &/ (\Delta E_t + \epsilon_1 + \epsilon_2 + \mu - \epsilon_f) \end{aligned} \quad (\text{B17})$$

$$\begin{aligned} \tilde{R}_8(\epsilon_1, \epsilon_2, \epsilon_3) &= [\mathcal{V}(\epsilon_1) R_6(\epsilon_2, \epsilon_3) \\ &+ \mathcal{V}(\epsilon_3) R_6(\epsilon_1, \epsilon_2) \\ &+ \mathcal{V}(\epsilon_2) \tilde{R}_5(\epsilon_1, \epsilon_3)] \\ &/ (\Delta E_t + \epsilon_1 + \epsilon_2 + \epsilon_3 - \epsilon_f) \end{aligned} \quad (\text{B18})$$

$$\begin{aligned} \tilde{R}_9(\epsilon_1, \epsilon_2, \epsilon_3) &= [\mathcal{V}(\epsilon_1) \tilde{R}_7(\epsilon_2, \epsilon_3) \\ &+ \mathcal{V}(\epsilon_2) \tilde{R}_7(\epsilon_1, \epsilon_3) \\ &+ \mathcal{V}(\epsilon_3) \tilde{R}_7(\epsilon_1, \epsilon_2)] \\ &/ (\Delta E_t + \epsilon_1 + \epsilon_2 + \epsilon_3 - \epsilon_f) \end{aligned} \quad (\text{B19})$$

$$\begin{aligned} \tilde{R}_{10}(\epsilon_1, \epsilon_2, E) &= \mathcal{V}(E) \tilde{R}_5(\epsilon_1, \epsilon_2) \\ &/ (\Delta E_t + \epsilon_1 + \epsilon_2 - E - \epsilon_f) \end{aligned} \quad (\text{B20})$$

$$\begin{aligned} R_{11}(\epsilon_1, \epsilon_2, E) &= \mathcal{V}(E) R_6(\epsilon_1, \epsilon_2) \\ &/ (\Delta E_t + \epsilon_1 + \epsilon_2 - E - \epsilon_f) \end{aligned} \quad (\text{B21})$$

$$\begin{aligned} \tilde{R}_{12}(\epsilon_1, \epsilon_2, E) &= \mathcal{V}(E) \tilde{R}_7(\epsilon_1, \epsilon_2) \\ &/ (\Delta E_t + \epsilon_1 + \epsilon_2 - E - \epsilon_f). \end{aligned} \quad (\text{B22})$$

where

$$\begin{aligned} \tilde{R}_2(\epsilon_1, \epsilon_2) &= \Theta(\epsilon_1 - \epsilon_2) R_2(\epsilon_1, \epsilon_2) \\ &+ \Theta(\epsilon_2 - \epsilon_1) R_2(\epsilon_2, \epsilon_1) \end{aligned} \quad (\text{B23})$$

$$\tilde{R}_5(\epsilon_1, \epsilon_2) = \Theta(\epsilon_1 - \epsilon_2) R_5(\epsilon_1, \epsilon_2)$$

$$+ \Theta(\epsilon_2 - \epsilon_1)R_5(\epsilon_2, \epsilon_1) \quad (B24)$$

$$\begin{aligned} \tilde{R}_7(\epsilon_1, \epsilon_2) &= \Theta(\epsilon_1 - \epsilon_2)R_7(\epsilon_1, \epsilon_2) \\ &+ \Theta(\epsilon_2 - \epsilon_1)R_7(\epsilon_2, \epsilon_1) \end{aligned} \quad (B25)$$

$$\begin{aligned} \tilde{R}_8(\epsilon_1, \epsilon_2, \epsilon_3) &= \Theta(\epsilon_1 - \epsilon_3)R_8(\epsilon_1, \epsilon_2, \epsilon_3) \\ &+ \Theta(\epsilon_2 - \epsilon_1)R_8(\epsilon_3, \epsilon_1, \epsilon_1) \end{aligned} \quad (B26)$$

$$\begin{aligned} \tilde{R}_9(\epsilon_1, \epsilon_2, \epsilon_3) &= \Theta(\epsilon_1 - \epsilon_2)\Theta(\epsilon_2 - \epsilon_3)R_9(\epsilon_1, \epsilon_2, \epsilon_3) \\ &+ \Theta(\epsilon_1 - \epsilon_3)\Theta(\epsilon_3 - \epsilon_2)R_9(\epsilon_1, \epsilon_3, \epsilon_2) \\ &+ \Theta(\epsilon_2 - \epsilon_1)\Theta(\epsilon_1 - \epsilon_3)R_9(\epsilon_2, \epsilon_1, \epsilon_3) \\ &+ \Theta(\epsilon_2 - \epsilon_3)\Theta(\epsilon_3 - \epsilon_1)R_9(\epsilon_2, \epsilon_3, \epsilon_1) \\ &+ \Theta(\epsilon_3 - \epsilon_1)\Theta(\epsilon_1 - \epsilon_2)R_9(\epsilon_3, \epsilon_1, \epsilon_2) \\ &+ \Theta(\epsilon_3 - \epsilon_2)\Theta(\epsilon_2 - \epsilon_1)R_9(\epsilon_3, \epsilon_2, \epsilon_1) \end{aligned} \quad (B27)$$

$$\begin{aligned} \tilde{R}_{10}(\epsilon_1, \epsilon_2, E) &= \Theta(\epsilon_1 - \epsilon_2)R_{10}(\epsilon_1, \epsilon_2, E) \\ &+ \Theta(\epsilon_2 - \epsilon_1)R_{10}(\epsilon_2, \epsilon_1, E) \end{aligned} \quad (B28)$$

$$\begin{aligned} \tilde{R}_{12}(\epsilon_1, \epsilon_2, E) &= \Theta(\epsilon_1 - \epsilon_2)R_{12}(\epsilon_1, \epsilon_2, E) \\ &+ \Theta(\epsilon_2 - \epsilon_1)R_{12}(\epsilon_2, \epsilon_1, E) . \end{aligned} \quad (B29)$$

and ΔE_t is the energy difference between the lowest magnetic state energy and the energy of the filled Fermi sea of the effective conduction band, Eq.(23) .

APPENDIX C: NUMERICS

A good illustration of the method is provided by the Anderson impurity model with a finite U [32,33]. In our case, putting in Eqs.(25), (26) $V = 0$, $\mu = U/2$ and taking $\mathcal{V}(\epsilon)$ from Figure 2 we obtain the variational principle equations for the singlet state of the symmetric Anderson model which represents the original Hubbard host, Eq. (2). We fix a value of ΔE and choose the following functions for starting the iterations: $r_2 = r_3 = 0$ and $r_1(\epsilon) = \sqrt{2}\mathcal{V}(\epsilon)/(\Delta E + \epsilon + U/2)$. Then, instead of the normalization we keep $r_0 = 1$ on all stages of iterations. The convergence is reached in a few steps and the minimal fixed point of the function f , Eq. (28), is found. The same method was applied to find ΔE_t for the symmetric Anderson model. We define $\Delta E_t - \Delta E_s = T_K^{AM}$ and find that $T_K^{AM}/D = 0.081, 0.025, 0.011, 0.003$ for $U/D = 1.0, 2.0, 2.5, 3.0$ respectively. We estimate the accuracy of above calculations as $\pm 10^{-4}$. We may check the credibility of our fixed point iterations by comparing the above values of T_K^{AM} with the width of the relevant central peak of the DOS in Figure 2. This width has to be proportional to T_K^{AM} [22] and one can see that it is a fairly good agreement indeed between widths ratios and ratios of T_K^{AM} for $U/D = 1, 2, 2.5$ while for the $U/D = 3$ the agreement is less good. The latter is expected because the relative error in this case much larger than in

three others. The other check is provided by the expected exponential dependence of T_K^{AM}/D upon U [1]. The latter is confirmed by an almost linear dependence between the calculated $\ln T_K^{AM}$ and U .

In calculating the singlet ground state energy of the two-impurity Hamiltonian H_{eff} we choose as the initial guess for the superposition in Eq. (24) the following functions:

$$\begin{aligned} r_4(\epsilon_1, \epsilon_2) &= r_5(\epsilon_1, \epsilon_2) = \delta(\epsilon_1)\delta(\epsilon_2) \\ r_i &= 0 \quad i \neq 4, 5 \end{aligned} \quad (C1)$$

The reason for this choice is that in the limit $V, \mathcal{V} \rightarrow 0$ (i.e. no interaction between the superposition states) the states $\phi_4(0, 0), \phi_5(0, 0)$ are the states with lowest energies and therefore the only ones which are occupied . The smaller V the faster the convergence of the iterations .

For similar reasons the initial guess for the lowest-lying triplet superposition is

$$\begin{aligned} R_5(\epsilon_1, \epsilon_2) &= R_6(\epsilon_1, \epsilon_2) = \delta(\epsilon_1)\delta(\epsilon_2) \\ r_i &= 0 \quad i \neq 4, 5 \end{aligned} \quad (C2)$$

An illustration of the iteration procedure for the singlet case is given in Figure 8 . As it is known ([30], [31], [32]) the variational wavefunction of the Anderson impurity model sharp varies in the vicinity of zero energy (i.e. Fermi energy). Therefore in order to achieve sufficiently accurate integration with a small number of mesh points we used the dense mesh in the vicinity of zero:

$$\epsilon_j = e^{\frac{j}{n_d} \ln(1+g/D)} - 1 \quad (C3)$$

where

$$\begin{aligned} 0 &\leq j \leq n_d \\ 0 &\leq g/D \ll 1 \end{aligned} \quad (C4)$$

g is the limit of the dense mesh and n_d is the number of dense mesh points . In the range $g < E \leq D$ the variational wavefunctions is usually smooth so we used a Gauss-Legendre mesh . The best g/D was found to be 10^{-3} .

As a criterion for convergence of the iteration procedure we took the inequality

$$J(i) = |f^{i+1}(\Delta E) - f^i(\Delta E)| < c \quad (C5)$$

where $f^i(\Delta E)$ is the value of the function $f(\Delta E)$, Eq. (28), in the i -th iteration and c is a small number. Surprisingly we found that the inequality

$$J(i+2)/J(i+1) - J(i+1)/J(i) < c \quad (C6)$$

holds for i which is much smaller as compared with a needed for the existence of the inequality in Eq. (C5). So after obtaining a convergence of the factor $J(i+1)/J(i)$ we calculated $f(\Delta E)$ by the geometric series sum rule

$$f(\Delta E) = \frac{f^i(\Delta E)}{1 - J(i+1)/J(i)} . \quad (C7)$$

The inequality $J(i+1)/J(i) > 1$ indicates divergence of the iterations .

-
- [1] A. M. Tsvelick and P. B. Wiegmann, *Adv. Phys.* **32**, 453 (1983).
- [2] A. C. Hewson, *The Kondo Problem to Heavy Fermions* (Cambridge University Press, Cambridge, 1993).
- [3] D. H. Lee and J. Toner, *Phys. Rev. Lett.* **69**, 3378 (1992).
- [4] A. Furusaki and N. Nagaosa, *Phys. Rev. Lett.* **72**, 892 (1994).
- [5] A. Schiller and K. Ingersent, *Phys. Rev. Lett.* **51**, 4676 (1995).
- [6] Y. M. Li, *Phys. Rev. B* **52**, R6979 (1995).
- [7] P. Phillips and N. Sandler, *Phys. Rev. B* **53**, 468 (1996).
- [8] A. Schiller and K. Ingersent, cond-mat 9609159 (1996).
- [9] We use here the notion of the Kondo effect as the generic one for all phenomena of a magnetic impurity in a metallic host.
- [10] T. Brugger, T. Schreiner, G. Roth, P. Adelman, and G. Czjzek, *Phys. Rev. Lett.* **71**, 2481 (1993).
- [11] P. Fulde, V. Zevin, and G. Zwicknagl, *Z. Phys. b* **92**, 133 (1993).
- [12] P. Fulde and V. Zevin, *Europhys. Lett.* **24**, 791, 1993.
- [13] S. Tornow, V. Zevin, and G. Zwicknagl, *Ann. Physik* **5**, 501, (1996).
- [14] T. Schork and P. Fulde, *Phys. Rev B* **50**, 1345, (1994).
- [15] G. Khaliullin and P. Fulde, *Phys. Rev. B* **52**, 9514 (1995).
- [16] T. Schork, *Phys. Rev. B* **53**, 5626 (1996).
- [17] S. Tornow, V. Zevin, and G. Zwicknagl, cond-mat/9701137 (1997)
- [18] The opposite effect was found in the paper: K. Itai and P. Fazekas, *Phys. Rev B* **54**, R752 (1996). Vertex corrections are not taking into account in this paper and that may be the reason of the discrepancy.
- [19] W. Metzner, and D. Vollhardt, *Phys. Rev. Lett.* **62**, 324 (1989).
- [20] E. Müller-Hartmann, *Z. Phys. B* **74**, 507 (1989)
- [21] D. Vollhardt, in *“Correlated Electron Systems”*, V. J. Emery, ed. (World Scientific) and references therein.
- [22] W. K. A. Georges, G. Kotliar W. Krauth and M. J. Rozenberg, *Rev. Mod. Phys.* (1996) and references therein.
- [23] A. Georges and G. Kotliar, *Phys. Rev. B* **45**, 6479 (1992).
- [24] M. Jarrell, *Phys. Rev. Lett.* **69**, 168 (1992).
- [25] Curves in Figure 2 produced with the the numeric data kindly sent to us by Dr. M. Rozenberg [26].
- [26] M. J. Rozenberg, G. Kotliar, and X. Y. Zhang, *Phys. Rev. B* **49**, 10 181, (1994).
- [27] B. Davidovitch, M. Sc. Thesis, The Hebrew University of Jerusalem, May 1996.
- [28] P. Coleman, *Phys. Rev. B* **35**, 5072, (1987).
- [29] N. E. Bickers, *RMP* **59**, 845 (1987).
- [30] C. M. Varma and Y. Yafet, *Phys. Rev. B* **13**, 2950, (1976).
- [31] O. Gunnarsson and K. Schönhammer, *Phys. Rev. B* **28**, 4315 , (1983).
- [32] O. Gunnarsson and K. Schönhammer, *Phys. Rev. B* **31**, 4815, (1985).
- [33] We applied this iteration scheme to the finite-U Anderson impurity of ref. [32] and easily obtained state occupancies and Kondo temperatures cited in ref. [32].
- [34] The meaning of the relevant magnetic states in the context of the variational approach to the Kondo effect is discussed in details in reference [32]. These are states which contribute to the Anderson impurity magnetic susceptibility where the Kondo scale appears. There are many other magnetic states with much lower energies but they are not connected by the impurity Zeeman interaction with the singlet ground state [32].
- [35] We note that in the non-interacting case the Kondo temperature as a function of the Anderson width Γ may have a maximum. This happens in a transitional region from the Kondo regime (where T_K increases exponentially with Γ) to the mixed valence one when a scale becomes of the order of ϵ_f^2/Γ (for $\Gamma \lesssim |\epsilon_f|$) and eventually transforms to $\sim \Gamma$ (for $\Gamma > |\epsilon_f|$) [1].

FIG. 1. A Bethe lattice with the impurity coupled to a lattice site.

FIG. 2. $2t(-ImG(\epsilon))$ versus $\epsilon/2t$ as calculated in [25] for the Hubbard model on Bethe lattice with the infinite coordination, $d \rightarrow \infty$. $U = 0;1;2;2.5;3;4$.

FIG. 3. Slave-boson and f-pseudofermions self-energies. The solid, dashed and wavy lines represent propagators for the c_0 -electron, f-pseudofermion and slave boson. The open circle denotes the bare hybridization interaction V while the filled square is two-particle vertex $\Gamma^U(12;34)$. a) The slave boson self-energy, $U = 0$. b) The f-pseudofermion self-energy, $U = 0$. c) and d) are additional contributions to self-energies a) and b) respectively for $U \neq 0$.

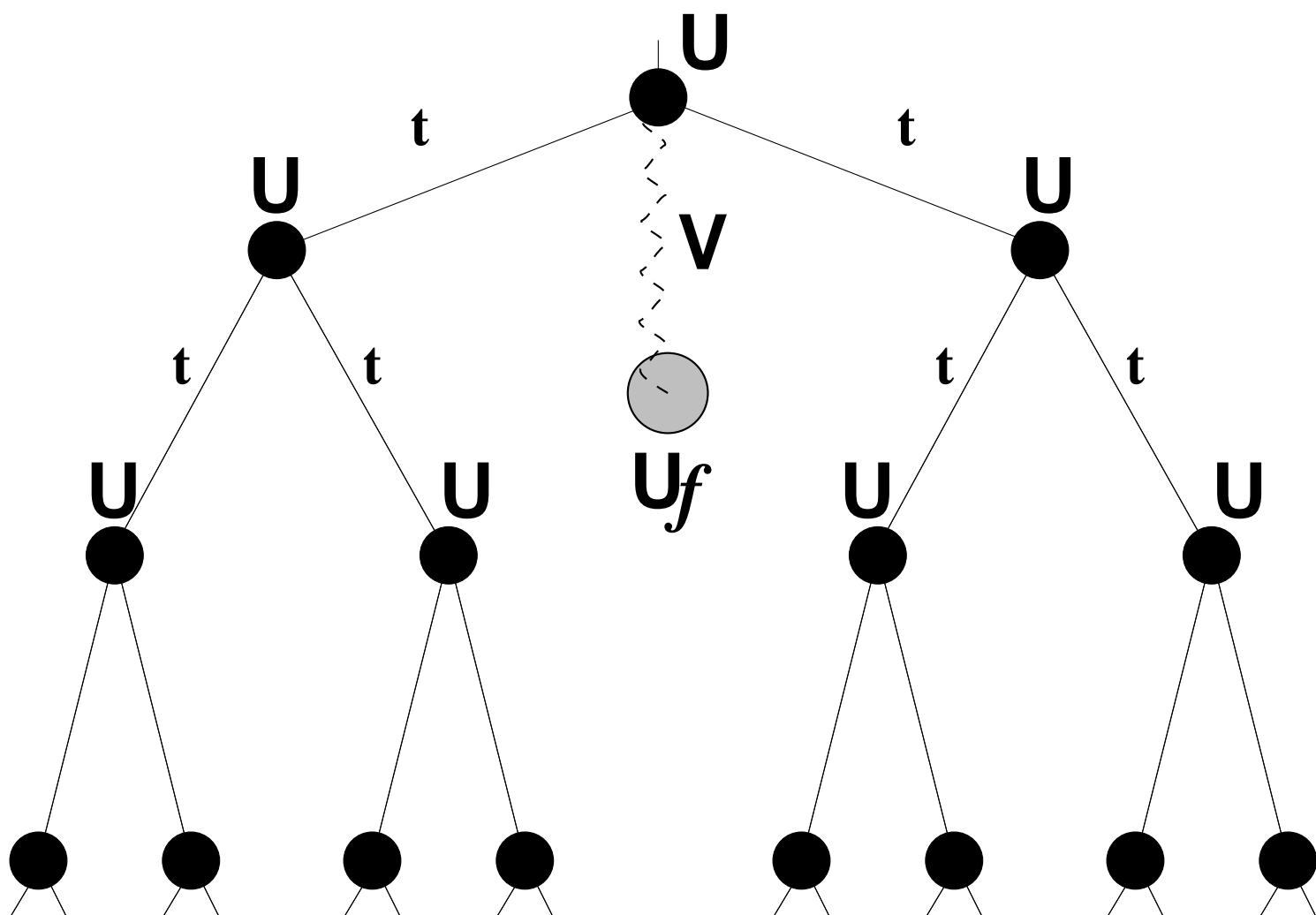
FIG. 4. An illustration of states ϕ_i which composite the singlet variational state, Eq. (24). Explanations of ϕ -states are in the text and in the Appendix A. Solid lines connect states which are coupled by the $V(\epsilon)$ -interaction and dashed lines are for the hybridization interaction V (see Eq. (23)).

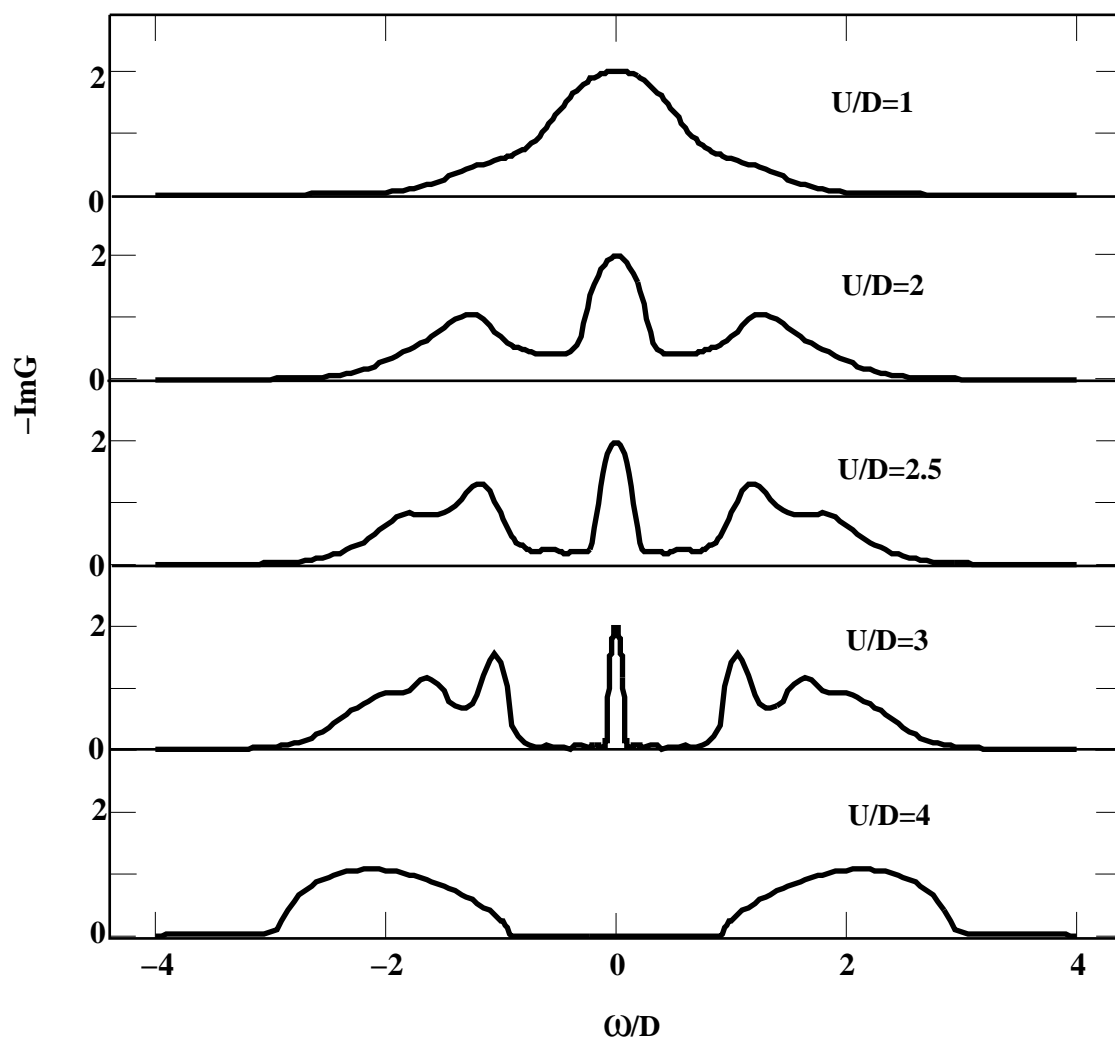
FIG. 5. T_K as a function of V^2 for $U = 1$ and $\epsilon_f = -0.3$ (upper curve) and -0.67 (low curve). All parameters in units of D . Curves are a guide to the eye.

FIG. 6. The same as in Figure 5 but for different values of U . Upper curve: $U/D = 2$, lower curve: $U/D = 2.5$. $\epsilon_f = -0.3$. Curves are a guide to the eye.

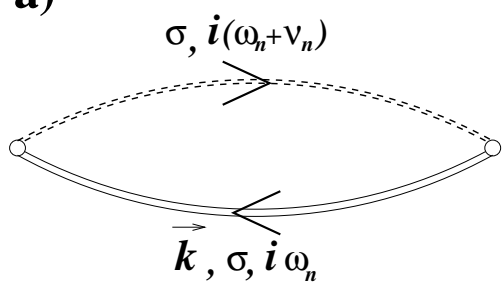
FIG. 7. T_K dependence on U for $\epsilon_f = -0.3$ and $V^2 = 0.01$.
The cross marks T_K from Eq. (21).

FIG. 8. An illustration of the iteration procedure for the singlet case.

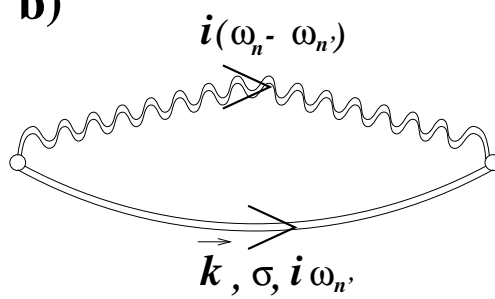




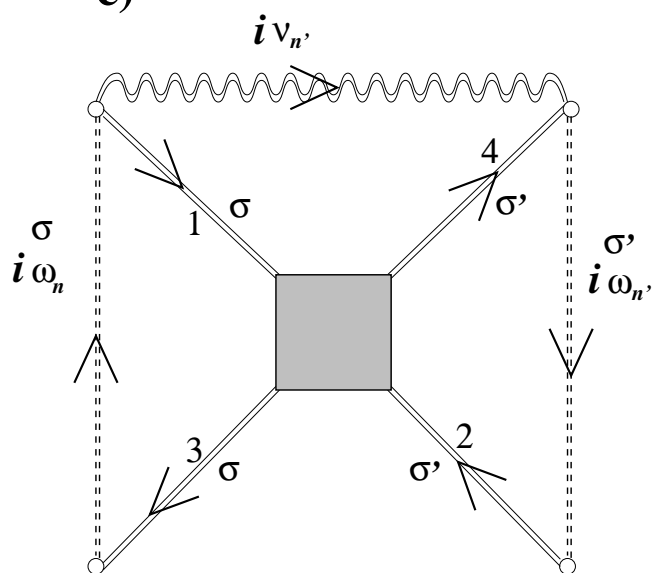
a)



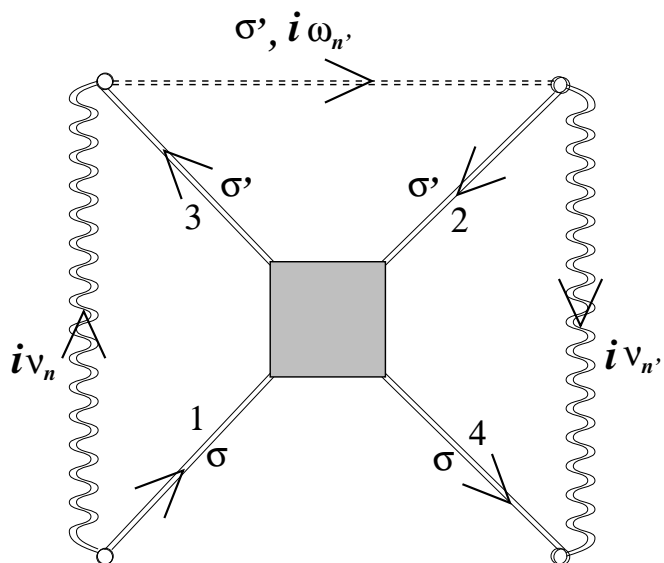
b)

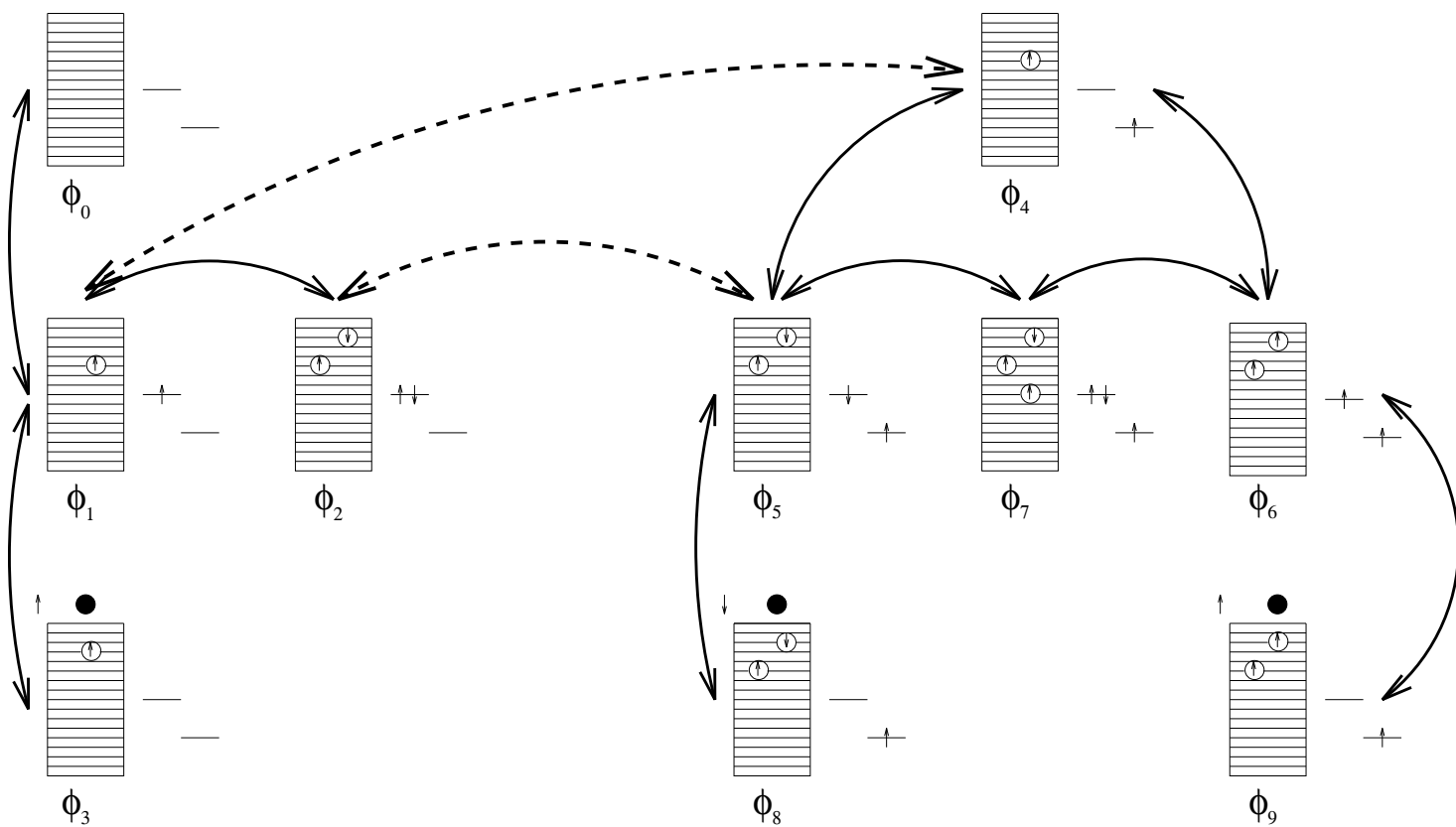


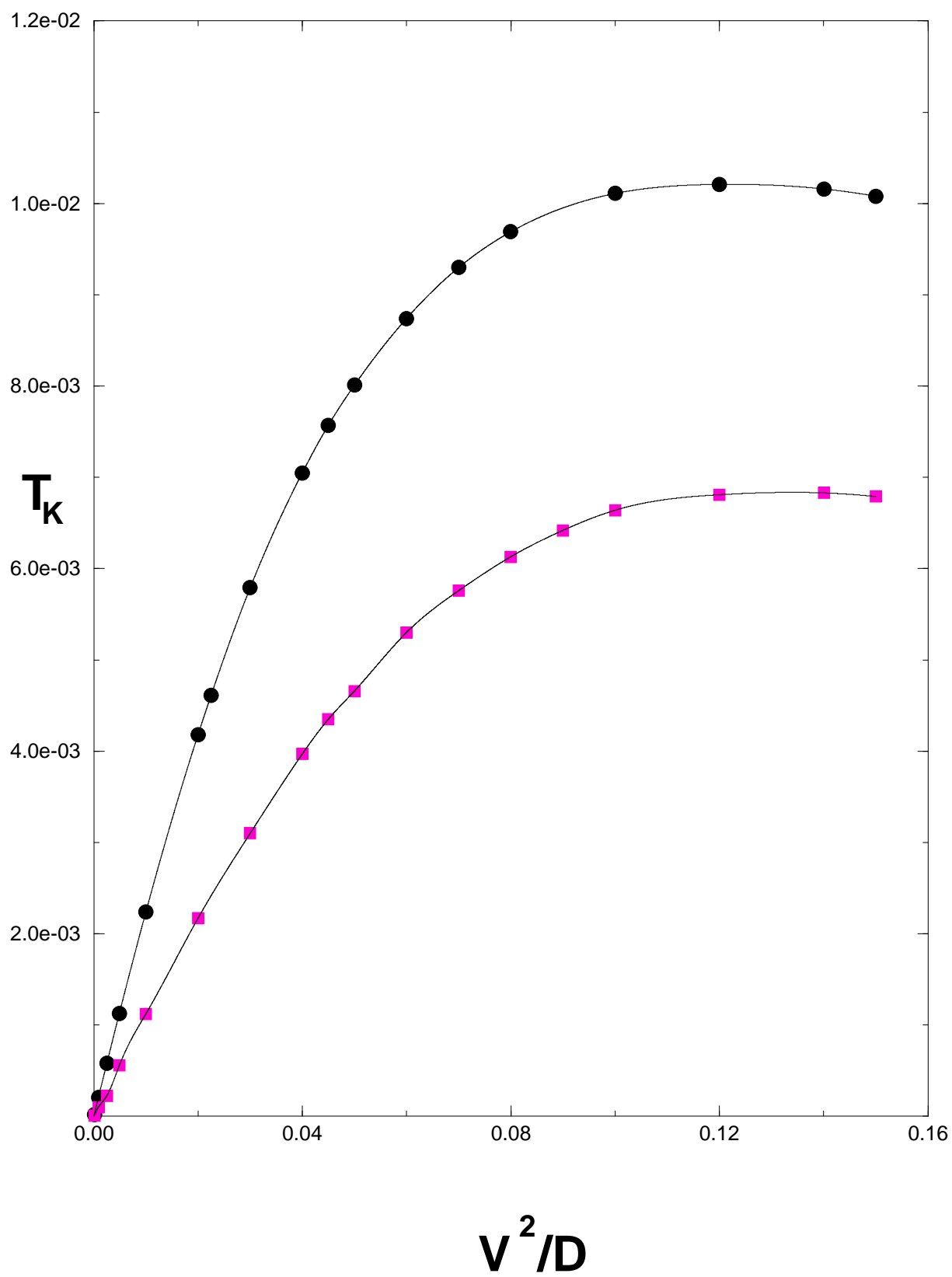
c)

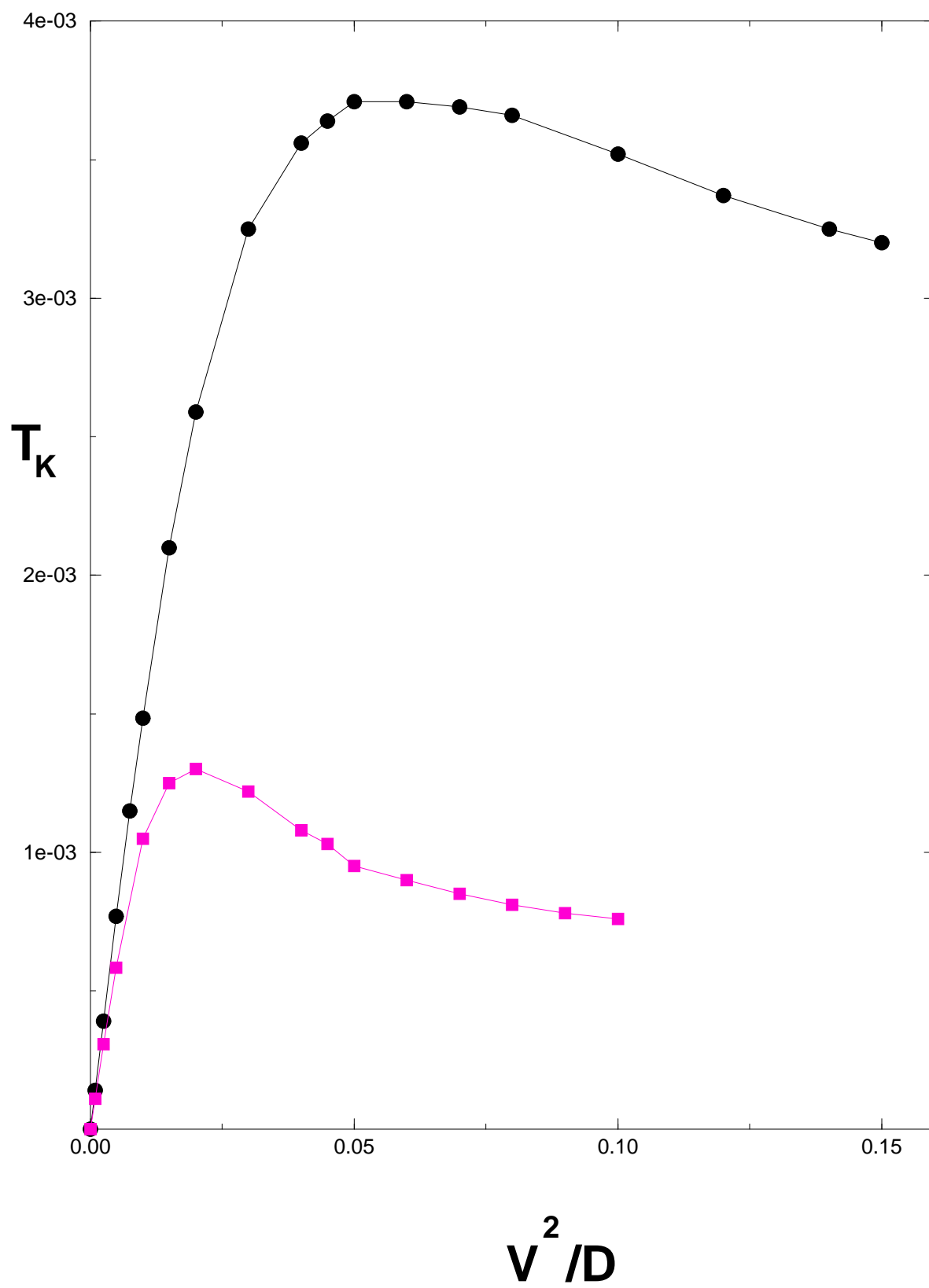


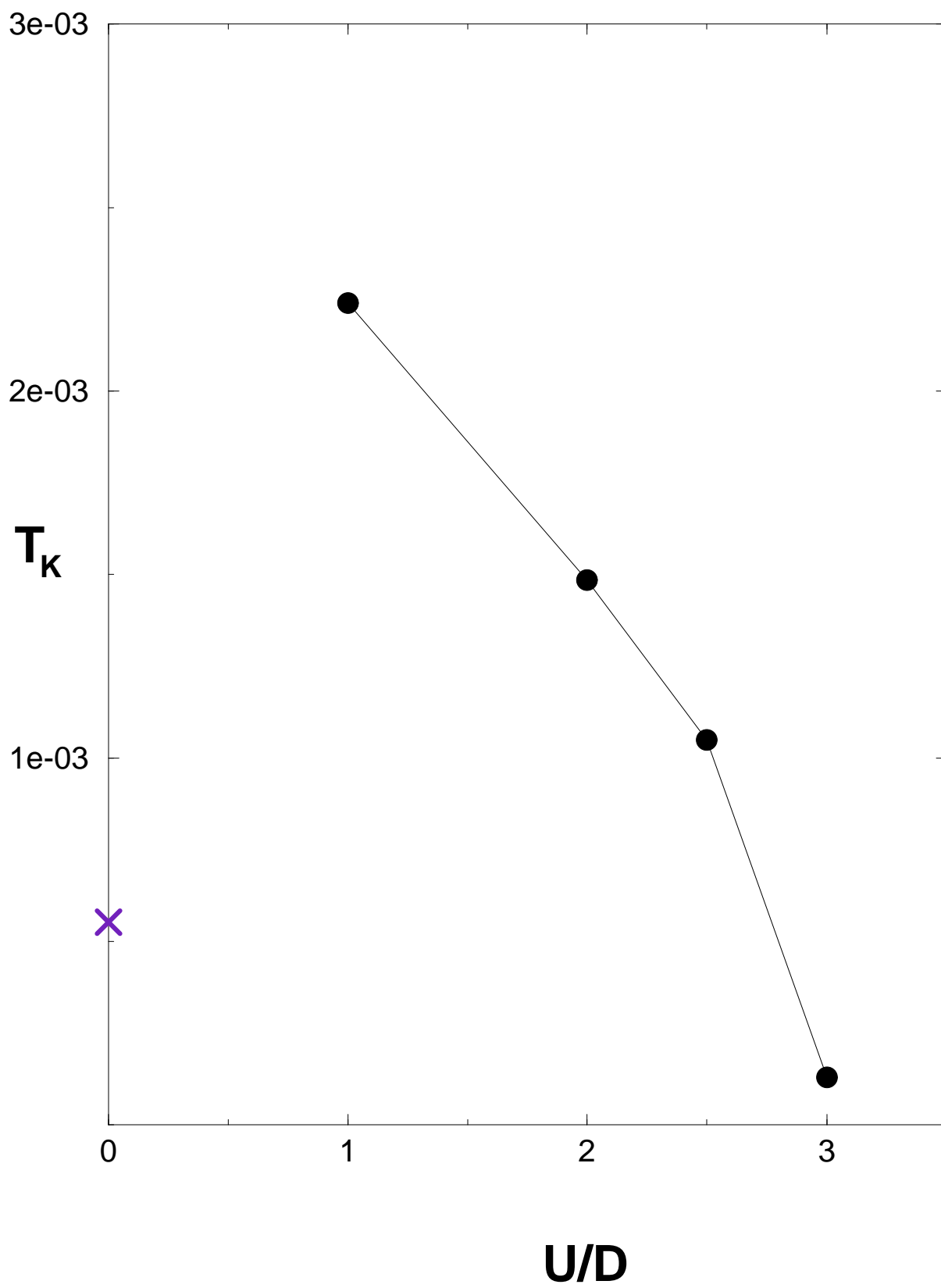
d)











$$r_5^{(i)} \quad r_6^{(i)} \quad \longrightarrow \rhd \quad r_7^{(i+1)} \quad r_4^{(i+1)} \quad r_8^{(i+1)} \quad r_9^{(i+1)}$$



$$r_4^{(i+1)} \quad \longrightarrow \rhd \quad r_1^{(i+1)}$$



$$r_1^{(i+1)} \quad r_5^{(i)} \quad \longrightarrow \rhd \quad r_2^{(i+1)}$$



$$r_1^{(i+1)} \quad \longrightarrow \rhd \quad r_0^{(i+1)} \quad r_3^{(i+1)}$$



$$r_2^{(i+1)} \quad r_4^{(i+1)} \quad r_7^{(i+1)} \quad r_8^{(i+1)} \quad r_9^{(i+1)} \quad \longrightarrow \rhd \quad r_5^{(i+1)} \quad r_6^{(i+1)}$$

$$r_5^{\Delta E} \quad r_6^{\Delta E} \quad \longrightarrow \rhd \quad \mathbf{f}(\Delta E)$$